Huiming Wang
Department of Engineering Mechanics,
Zhejiang University,
Hangzhou 310027, P.R. China;
School of Engineering
and Applied Sciences,
Kavli Institute for Nanobio Science
and Technology,
Harvard University,
Cambridge, MA 02138

Shengqiang Cai
School of Engineering
and Applied Sciences,
Kavli Institute for Nanobio
Science and Technology,
Harvard University,
Cambridge, MA 02138

Federico Carpi
Interdepartmental Research Centre "E. Piaggio,"
School of Engineering,
University of Pisa,
Pisa 56100, Italy;
Technology & Life Institute,
Pisa 56100, Italy
e-mail: f.carpi@ing.unipi.it

Zhigang Suo
School of Engineering
and Applied Sciences,
Kavli Institute for Nanobio
Science and Technology,
Harvard University,
Cambridge, MA 02138
e-mail: suo@seas.harvard.edu

Computational Model of Hydrostatically Coupled Dielectric Elastomer Actuators

A hydrostatically coupled dielectric elastomer (HCDE) actuator consists of two membranes of a dielectric elastomer, clamped with rigid circular rings. Confined between the membranes is a fixed volume of a fluid, which couples the movements of the two membranes when a voltage or a force is applied. This paper presents a computational model of the actuator, assuming that the membranes are neo-Hookean, capable of large and axisymmetric deformation. The voltage-induced deformation is described by the model of ideal dielectric elastomer. The force is applied by pressing a rigid flat punch onto one of the membranes over an area of contact. The computational predictions agree well with experimental data. The model can be used to explore nonlinear behavior of the HCDE actuators. [DOI: 10.1115/1.4005885]

1 Introduction

The recent decade has seen the intense development of dielectric elastomers as materials for muscle-like transducers [1–5]. The principle of operation invokes a simple and robust mechanism of electromechanical coupling. Subject to voltage, a membrane of a dielectric elastomer reduces in thickness and expands in area. Attributes include voltage-actuated large deformation, light weight, fast response, ease of processing, and low cost. Promising applications range from haptics, adaptive optics to energy harvesting [2–4]. A commercial product with significant potential has just been released [6].

Mimicking muscles and bones, muscle-like transducers are often structures of tensegrity, with membranes of soft materials in tension, and members of hard materials in compression. The tension enables the membranes to provide some rigidity to the structures, while the softness enables the membranes to actuate large configurational change of the structures [7]. The large deformation may be accompanied with rich nonlinear behavior of instability, which can be harnessed to enhance dramatically the performance of transducers [8–11]. The development of the theory of dielectric elastomers presents a unique opportunity in mechanics [5].

Recently, a new class of actuators based on dielectric elastomers have been described, named HCDE actuators [12–14]. Such an actuator consists of two membranes of a dielectric elastomer, clamped by rigid circular rings (Fig. 1). The bottom membrane is sandwiched between soft electrodes and is referred to as the active membrane. The top membrane can bear an external force and is referred to as the passive membrane. Confined between the two membranes is a fixed volume of a fluid. In the absence of the voltage and the force, Fig. 1(*a*), the actuator is in the rest state. When a voltage is applied between the electrodes, Fig. 1(*b*), the bottom membrane expands its area and deforms downward. The volume of the fluid is conserved, which couples the deformation of the two membranes, producing a push–pull action.

The HCDE actuator is a structure of tensegrity: the membranes are in tension, while the rings and the fluid are in compression. The inclusion of the fluid in the structure imparts additional properties. The fluid couples the movements of the two membranes but separates their functions. One membrane interfaces with the external force and the other actuate the movement by voltage. If desired, the two functions can be realized by membranes located far apart.

The HCDE actuators are being developed as haptic displays, as well as wearable cutaneous stimulators [12–14]. This development targets significant applications, such as tactile feedback for mobile gaming [6] and Braille displays [15]. Within this context, the HCDE actuators offer two attractive features [12–14]. First, one can touch the passive membrane without being exposed to the high voltage that drives the active membrane. Second, local

Contributed by the Applied Mechanics Division of ASME for publication in the Journal of Applied Mechanics. Manuscript received July 2, 2011; final manuscript received October 13, 2011; accepted manuscript posted February 13, 2012; published online April 4, 2012. Assoc. Editor: Huajian Gao.

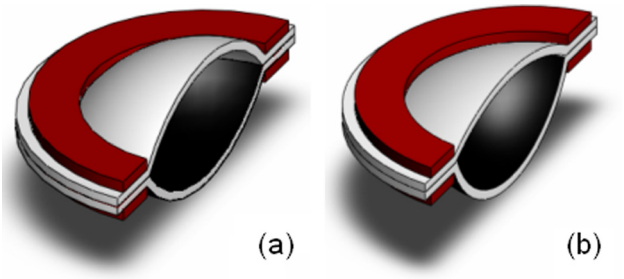

Fig. 1 Sectional views of a HCDE actuator. Two membranes of a dielectric elastomer are clamped by rigid circular rings. The bottom membrane is sandwiched between soft electrodes, which are connected to a voltage source. Confined in between the membranes is a certain volume of a fluid. (*a*) When the voltage is off, the actuator is in the rest state. (*b*) When the voltage in on, the bottom membrane expands in area and moves downward, pulling the top membrane down through the coupling fluid.

distortion of the passive membrane caused by the external force is redistributed by the fluid, and is smoothly transferred to the active membrane. This fact increases the electrical robustness of the device. If the mechanical load were applied directly on the active membrane, a local perturbation could lead to premature electrical breakdown.

To develop the HCDE actuators further, a computational model is desired. Anticipated uses of the computational model include predicting strokes and blocking forces, optimizing them by surveying the parameter space, analyzing inhomogeneous fields to avert various modes of failure. While efforts have been made to model curved membranes of dielectric elastomers under mechanical and electrical loads [16–20], no model has dealt with the HCDE actuators.

This paper presents a computational model of the HCDE actuators. We formulate the governing equations on the basis of a nonlinear field theory of deformable dielectrics. The membranes are assumed to be neo-Hookean, capable of large and axisymmetric deformation. The voltage-induced deformation is described by the model of ideal dielectric elastomers. The force is applied by pressing a rigid flat punch against one of the membranes. A computational procedure is described to account for the incompressible fluid and the membrane-punch contact. Computational results are compared with experimental data and are used to discuss basic characteristics of the HCDE actuators.

2 Experiment

Figure 2 sketches the experiment that characterizes HCDE actuators [14]. When an actuator was in the rest state, a rigid flat punch was brought to touch the top membrane with negligible force (Fig. 2(*a*)). When a voltage was applied to the bottom membrane, both membranes moved downward (Fig. 2(*b*)). The free stroke was measured as the distance to bring the punch to touch the top membrane again with negligible force (Fig. 2(*c*)). When the voltage was turned off and the punch was maintained in position, the top membrane pushed the punch with a blocking force, over a region of contact (Fig. 2(*d*)). The experimental data used to validate the computational model are extracted from Ref. [14]. They refer to actuators assembled with the materials and the parameters listed in Table 1.

Table 1 Materials and parameters of the HCDE actuator used to validate the model

Dielectric elastomer membrane	3M VHB 4910 acrylic
Compliant electrode material	Carbon grease
Coupling fluid	Silicone grease
Biaxial membrane prestrain	300%
Prestretched membrane thickness	60.6 μm
Base radius	10 mm
Apical height	1.78 mm
Radius of curvature	29 mm
Internal volume	563.53 mm^3

3 Governing Equations and Boundary Conditions

This section presents the governing equations and boundary conditions. The nonlinear field theory of elastic dielectrics dates back to the classic works of Toupin [21], Eringen [22], and Tiersten [23]. The theory has been re-examined in recent years in light of the intense development of dielectric elastomer transducers [16,24–31]. Here, we focus on membranes of dielectric elastomers undergoing axisymmetric deformation [16–20].

The computational model is illustrated with several states of the membranes in Fig. 3. In the undeformed state, Fig. 3(*a*), two circular membranes, radius A, and thickness H, lie on a plane. In the prestretched state, Fig. 3(*b*), the membranes are clamped by rigid rings of radius a. In the fluid-filled rest state, Fig. 3(*c*), a fluid of volume $2V_0$ is injected between the two membranes, the pressure in the fluid relative to the pressure in the ambient is p_0, and the apex of each membrane reaches the height h_0. In the actuated state, Fig. 3(*d*), a voltage Φ is applied through the thickness of the bottom membrane, the area of the bottom membrane expands, and the apex of the top membrane is pulled down to the height h. In the blocked state, Fig. 3(*e*), the voltage on the bottom is turned off, and a rigid flat punch presses the top membrane with a force F over a contact of radius b. Both the voltage and the force change the pressure in the fluid.

We first examine the kinematics of the actuator. The undeformed state, Fig. 3(*a*), is used as the reference state, in which we

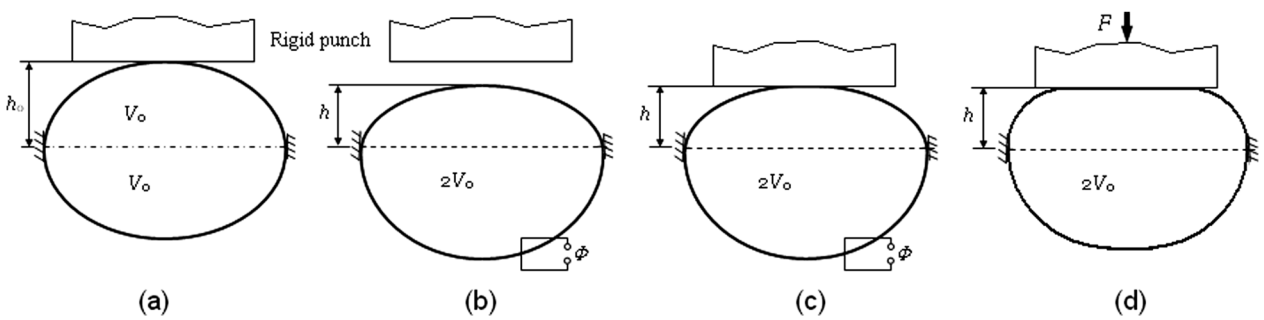

Fig. 2 Experiment to characterize the HCDE actuator. (*a*) While the actuator is in the rest state, a rigid flat punch is brought to touch the top membrane with negligible force. (*b*) When the bottom membrane is subject to voltage, both membranes move downward. (*c*) While the voltage is on, the rigid punch is brought to touch the top membrane with negligible force, and the displacement of the punch defines the free stroke. (*d*) The voltage is turned off while the punch is fixed in position, the punch presses the top membrane over an area of contact at a certain blocking force.

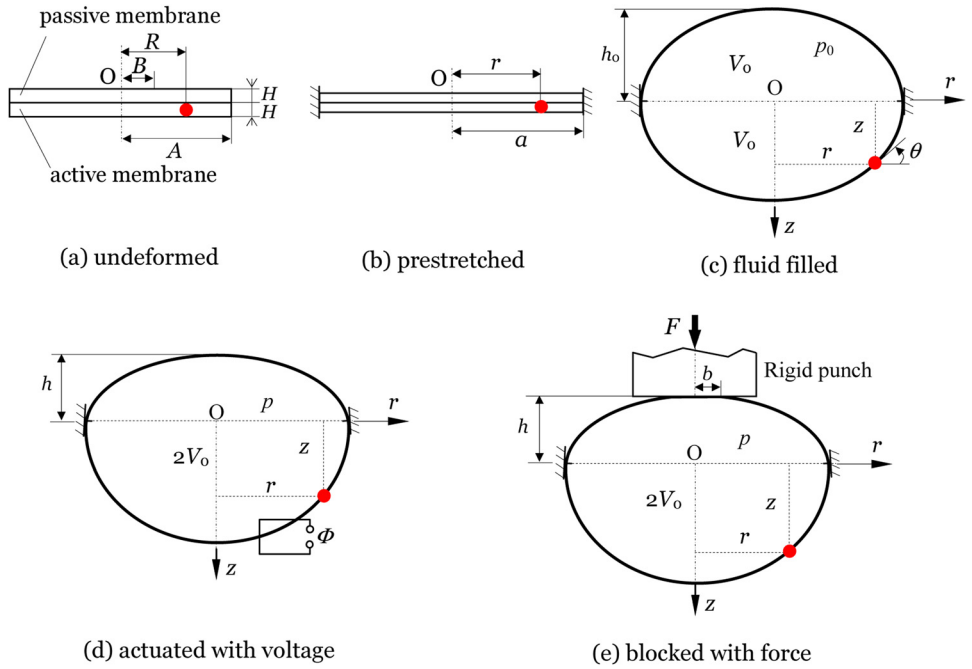

Fig. 3 Schematics of states used to describe the computational model. In each state, the position of a particular material particle has been identified by a circular dot.

label each material particle by its radial coordinate R. The membranes are assumed to deform into an axisymmetric shape (Fig. 3(*c*)–3(*e*)). Let the coordinate z coincide with the axis of symmetry, the coordinate r coincide with a radial direction, and the plane $z = 0$ coincide with the plane of the rigid rings. In a deformed state, the material particle R takes the position of coordinates z and r. The functions $z(R)$ and $r(R)$ of either membrane characterize its deformed state. The determination of the two functions for both membranes is an object of the computational model.

Consider a material element of one of the membranes, between two particles R and $R + dR$. When the membrane is in a deformed state, the particle R takes the position of coordinates $z(R)$ and $r(R)$, while the particle $R + dR$ takes the position of coordinates $z(R + dR)$ and $r(R + dR)$. In the undeformed state, the material element is a straight segment, length dR. In the deformed state, the material element becomes a curved segment, length $\lambda_1 dR$, where λ_1 is the longitudinal stretch. In a curved state, let $\theta(R)$ be the slope of a membrane at material particle R. Write $dr = r(R + dR) - r(R)$, so that

$$\frac{dr}{dR} = \lambda_1 \cos\theta \tag{1}$$

Similarly, write $dz = z(R + dR) - z(R)$, so that

$$\frac{dz}{dR} = -\lambda_1 \sin\theta \tag{2}$$

Consider, in the undeformed state, a circle of material particles, perimeter $2\pi R$. In the deformed state, these material particles occupy a circle of positions, perimeter $2\pi r$. The deformation causes the latitudinal stretch $\lambda_2 = r/R$. When the membranes are in the prestretched state, Fig. 3(*b*), both stretches are homogeneous in the membranes $\lambda_1 = \lambda_2 = a/A$. When the membranes are in a curved state, Figs. 3(*c*)–3(*e*), however, the stretches are inhomogeneous in the membranes, and are described by functions $\lambda_1(R)$ and $\lambda_2(R)$.

We next study the mechanical equilibrium. Consider an element of a membrane located at position R in the reference state. In a deformed state, the element is subject to tensile stresses in the longitudinal and latitudinal directions, while the stress in the direction normal to the membrane is negligible. Let $s_1(R)$ be the longitudinal nominal stress and $s_2(R)$ the latitudinal nominal stress. Figure 4 sketches free-body diagrams. In the undeformed state, Fig. 4(*a*), consider an annulus of the membrane between

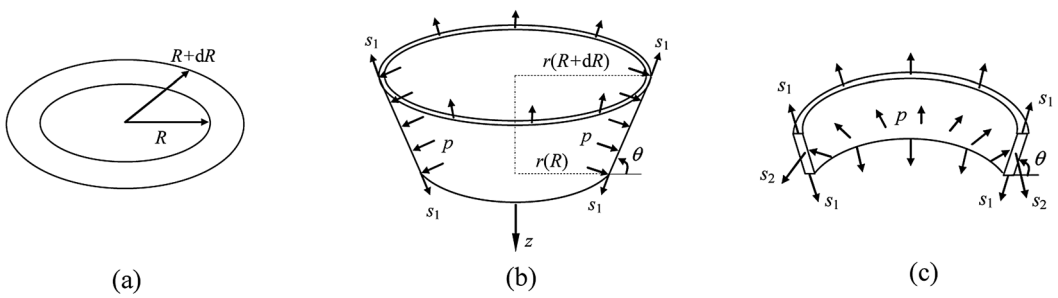

Fig. 4 Free-body diagrams to describe the mechanical equilibrium of a membrane. (*a*) In the undeformed state of the membrane, imagine an annulus, radii *R* and *R* + *dR*. (*b*) In a deformed state, the annulus becomes an axisymmetric band. The pressure on the face of the band is balanced by the longitudinal stress on the rims of the band. (*c*) Balance the pressure, the longitudinal stress, and the latitudinal stress in a half of the band.

R and $R+dR$. In the deformed state, Fig. 4(*b*), the annulus deforms into an axisymmetric band in three dimensions. Acting on the band are the pressure p on the face of the band and the longitudinal stresses on the rims of the band. Balancing these forces in the z-direction, we obtain that

$$\frac{d}{dR}(HRs_1 \sin\theta) = \lambda_1\lambda_2 Rp \cos\theta \tag{3}$$

We next examine the free-body diagram of a half of the band, Fig. 4(*c*). Balancing the forces acting on the half band in the latitudinal direction, we obtain that

$$\frac{d}{dR}(HRs_1 \cos\theta) + \lambda_1\lambda_2 Rp \sin\theta = s_2 H \tag{4}$$

The electrical equilibrium is much easier to describe. When the two electrodes on the active membrane are connected to a voltage source, an electric current commences, charging the membrane. In equilibrium, the electric current stops, and the voltage between the two electrodes equals the voltage of the source, Φ. Define the nominal electric field in the membrane by $\tilde{E} = \Phi/H$. Define the nominal electric displacement $\tilde{D}(R)$ by the electric charge on an element of an electrode in the deformed state divided by the area of the element in the undeformed state.

We next consider the boundary conditions. The rigid rings clamp the membranes, so that the edge of the membranes does not move

$$r(A) = a, \quad z(A) = 0 \tag{5}$$

At the apex of the active membrane, symmetry requires that

$$\theta(0) = 0, \quad r(0) = 0 \tag{6}$$

For the passive membrane blocked by the punch, denote the radius of contact by B in the reference state, and b in the deformed state. The punch and the membrane are taken to be free of friction and adhesion, so that the circular region of the membrane in contact with the punch is in a state of homogenous, equal-biaxial stretches

$$\lambda_1(R) = \lambda_2(R) = b/B, \quad \text{for} \quad R < B \tag{7}$$

The two components of the nominal stresses are also equal and can be determined by the stress–stretch relation. For example, when the elasticity of the membrane is described by the neo-Hookean model, as in Sec. 4, the stresses in the membrane within the region of contact are given by

$$s_1(R) = s_2(R) = \mu\left[\left(\frac{b}{B}\right) - \left(\frac{b}{B}\right)^{-5}\right], \quad \text{for} \quad R < B \tag{8}$$

For the curved part of the passive membrane, the following conditions of continuity are applied at the boundary of the contact:

$$r(B) = b \tag{9}$$

$$z(B) = h \tag{10}$$

$$\theta(B) = 0 \tag{11}$$

$$s_1(B) = \mu\left[\left(\frac{b}{B}\right) - \left(\frac{b}{B}\right)^{-5}\right] \tag{12}$$

Conditions (11) and (12) apply when the punch and the membrane are free of friction and adhesion [32].

Finally, consider the membrane in the region of contact as a free-body diagram. The upper surface of the region is subject to the force from the punch, F. The lower surface of the region is subject to the pressure from the fluid, p. Because $\theta(B) = 0$, the longitudinal stress on the edge of the region is in the horizontal direction. Balancing the force from the punch and the pressure from the fluid, we obtain that

$$F = \pi b^2 p \tag{13}$$

4 Material Model

Material models of electromechanical coupling have been reviewed recently [5]. Here, we outline the specific model used in the present work. A dielectric elastomer is a thermodynamic system, taken to be held at a constant temperature. In a state of equilibrium, an element of the dielectric elastomer is characterized by three independent kinematic variables: $\lambda_1, \lambda_2, \tilde{D}$. Let W be the nominal density of the Helmholtz free energy—that is, the free energy of an element of the dielectric elastomer in the current state divided by the volume of the element in the reference state. As a material model, we specify the density of the Helmholtz free energy W as a function of the three kinematic variables

$$W = W(\lambda_1, \lambda_2, \tilde{D}) \tag{14}$$

Associated with the variations of the kinematic variables, the free energy varies by

$$\delta W = \frac{\partial W(\lambda_1, \lambda_2, \tilde{D})}{\partial \lambda_1}\delta\lambda_1 + \frac{\partial W(\lambda_1, \lambda_2, \tilde{D})}{\partial \lambda_2}\delta\lambda_2 + \frac{\partial W(\lambda_1, \lambda_2, \tilde{D})}{\partial \tilde{D}}\delta\tilde{D} \tag{15}$$

The element of the dielectric elastomer is subject to the stresses and electric field. In a state of equilibrium, the change in the Helmholtz free energy equals the sum of the work done by the stresses and the work done by the electric field

$$\delta W = s_1\delta\lambda_1 + s_2\delta\lambda_2 + \tilde{E}\delta\tilde{D} \tag{16}$$

The longitudinal nominal stress, the latitudinal nominal, and the nominal electric field are work-conjugate to the three kinematic variables. Thermodynamics dictates that the condition of equilibrium (16) should hold for arbitrary small variations $\delta\lambda_1, \delta\lambda_2, \delta\tilde{D}$ from the state of equilibrium.

A comparison of Eqs. (15) and (16) gives that

$$\left[s_1 - \frac{\partial W(\lambda_1, \lambda_2, \tilde{D})}{\partial \lambda_1}\right]\delta\lambda_1 + \left[s_2 - \frac{\partial W(\lambda_1, \lambda_2, \tilde{D})}{\partial \lambda_2}\right]\delta\lambda_2 + \left[\tilde{E} - \frac{\partial W(\lambda_1, \lambda_2, \tilde{D})}{\partial \tilde{D}}\right]\delta\tilde{D} = 0 \tag{17}$$

Because $\delta\lambda_1, \delta\lambda_2, \delta\tilde{D}$ are independent variations, the condition of equilibrium (17) is equivalent to three equations of state

$$s_1 = \frac{\partial W(\lambda_1, \lambda_2, \tilde{D})}{\partial \lambda_1} \tag{18}$$

$$s_2 = \frac{\partial W(\lambda_1, \lambda_2, \tilde{D})}{\partial \lambda_2} \tag{19}$$

$$\tilde{E} = \frac{\partial W(\lambda_1, \lambda_2, \tilde{D})}{\partial \tilde{D}} \tag{20}$$

The equations of state (18)–(20) take an explicit form once the free energy function $W(\lambda_1, \lambda_2, \tilde{D})$ is prescribed.

To prescribe a specific form of the function, $W(\lambda_1, \lambda_2, \tilde{D})$, we adopt the model of ideal dielectric elastomers [29]. This model assumes that the dielectric behavior of the elastomer is liquid-like,

and unaffected by deformation. This assumption is motivated as follows. An elastomer is a three-dimensional network of long and flexible polymers, held together by crosslinks. Each polymer chain consists of a large number of monomers. Consequently, the crosslinks negligibly affect the polarization of the monomers—that is, the elastomer can polarize nearly as freely as a polymer melt. This molecular picture is consistent with the following experimental observation: the permittivity changes by only a few percent when a membrane of an elastomer is stretched to increase the area 25 times [33].

The model of ideal dielectric elastomers assumes that the dielectric behavior of an elastomer is exactly the same as that of a polymer melt. The true electric displacement D is linear in the true electric field E, namely, $D = \varepsilon E$, with the permittivity ε being independent of the stretches. Furthermore, the elastomer is assumed to be incompressible, so that the stretch in the thickness direction of the membrane, λ_3, related to λ_1 and λ_2 as $\lambda_3 = 1/\lambda_1\lambda_2$. The true electric field relates to the nominal electric field as $E = \lambda_1\lambda_2\tilde{E}$. The true electric displacement relates to the nominal electric displacement as $D = \tilde{D}/(\lambda_1\lambda_2)$. We rewrite $D = \varepsilon E$ in terms of the nominal electric field and the nominal electric displacement

$$\tilde{E} = \frac{\tilde{D}}{\varepsilon}\lambda_1^{-2}\lambda_2^{-2} \tag{21}$$

Inserting Eq. (21) into Eq. (20) and integrating with respect to $\tilde{D}$, we obtain that

$$W(\lambda_1, \lambda_2, \tilde{D}) = W_{\text{stretch}}(\lambda_1, \lambda_2) + \frac{\tilde{D}^2}{2\varepsilon}\lambda_1^{-2}\lambda_2^{-2} \tag{22}$$

The constant of integration, $W_{\text{stretch}}(\lambda_1, \lambda_2)$, represents the free energy associated with the stretching of the elastomer. Equation (22) is readily interpreted. In the model of dielectric elastomers, the free energy of the elastomer is the sum of that due to stretching the network and that due to polarization. The electromechanical coupling only appears in the second term in (22), and is caused entirely by the geometric effect discussed above.

The free energy of stretching $W_{\text{stretch}}(\lambda_1, \lambda_2)$ can be taken from the large repertoire in the literature on rubber elasticity [34]. For simplicity, here we adopt the neo-Hookean model

$$W_{\text{stretch}}(\lambda_1, \lambda_2) = \frac{\mu}{2}\left(\lambda_1^2 + \lambda_2^2 + \lambda_1^{-2}\lambda_2^{-2} - 3\right) \tag{23}$$

where μ is the small strain shear modulus. Inserting Eqs. (22) and (23) into Eqs. (18) and (19), we obtain that

$$s_1 = \mu\left(\lambda_1 - \lambda_1^{-3}\lambda_2^{-2}\right) - \frac{\tilde{D}^2}{\varepsilon}\lambda_1^{-3}\lambda_2^{-2} \tag{24}$$

$$s_2 = \mu\left(\lambda_2 - \lambda_1^{-2}\lambda_2^{-3}\right) - \frac{\tilde{D}^2}{\varepsilon}\lambda_1^{-2}\lambda_2^{-3} \tag{25}$$

For passive membrane, the stress–stretch relations are obtained by setting $\tilde{D} = 0$.

Incidentally, the true stresses relate to the nominal stresses as $\sigma_1 = \lambda_1 s_1$ and $\sigma_2 = \lambda_2 s_2$. In terms of the true quantities, Eqs. (18) and (19) take the form

$$\sigma_1 = \lambda_1\frac{\partial W_{\text{stretch}}(\lambda_1, \lambda_2)}{\partial\lambda_1} - \varepsilon E^2 \tag{26}$$

$$\sigma_2 = \lambda_2\frac{\partial W_{\text{stretch}}(\lambda_1, \lambda_2)}{\partial\lambda_1} - \varepsilon E^2 \tag{27}$$

The term εE^2 is commonly called the Maxwell stress. As evident from the above discussion, Eqs. (26) and (27) are applicable only to ideal dielectric elastomers. The model of ideal dielectric elastomers is nearly exclusively used in previous analysis of dielectric elastomers [16,24–31,35–40]. Further discussion of the model of ideal dielectric elastomers and other material models can be found in Ref. [5].

5 Notes on Computational Method

The governing equations presented in Sec. 3 can be written as a set of first-order ordinary differential equations for the four functions: $r(R)$, $z(R)$, $\theta(R)$, and $\lambda_1(R)$. Equations (1) and (2) are already in the desired form. A combination of Eqs. (3) and (4), along with the material model, gives that

$$\frac{d\theta}{dR} = -\frac{s_2}{s_1}\frac{\sin\theta}{R} + \frac{\lambda_1\lambda_2}{s_1}\frac{p}{H} \tag{28}$$

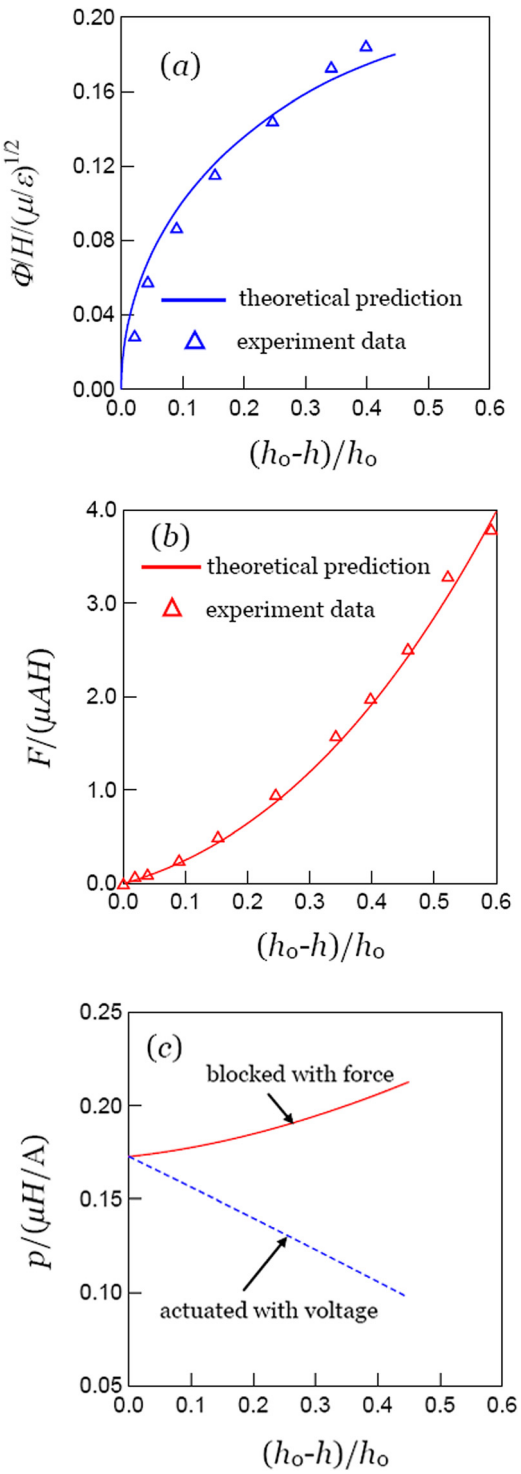

Fig. 5 (*a*) Voltage, (*b*) force, and (*c*) pressure as functions of the apical displacement. The experimental data are extracted from Ref. [14].

$$\frac{d\lambda_1}{dR}=\frac{s_2\cos\theta-s_1-2\left(\mu\lambda_1^{-3}\lambda_2^{-3}-\varepsilon\tilde{E}^2\lambda_1\lambda_2\right)\left(\lambda_1\cos\theta-\lambda_2\right)}{R\mu\left(1+3\lambda_1^{-4}\lambda_2^{-2}\right)-R\varepsilon\tilde{E}^2\lambda_2^2} \tag{29}$$

where $\tilde{E}=\Phi/H$ for the active membrane and $\tilde{E}=0$ for the passive membrane. The stresses on the right-hand side of Eqs. (28) and (29) are related to λ_1 and λ_2 through the material model, and the latitudinal stress is related to the function $r(R)$ by the

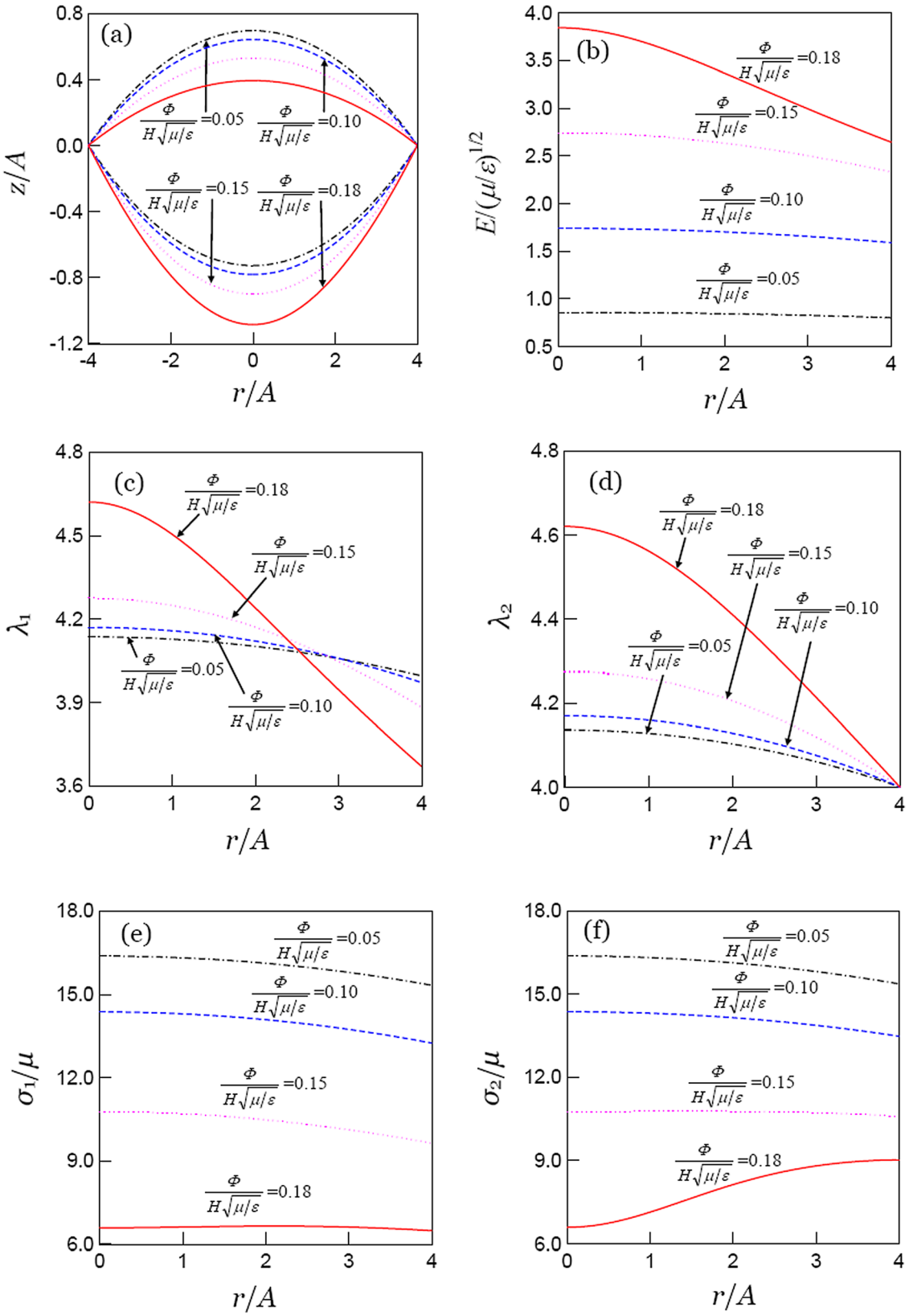

Fig. 6 Distribution of various fields in the active membrane at several values of the voltage. (*a*) Deformed shapes of the actuator. (*b*) True electric field. (*c*) Longitudinal stretch. (*d*) Latitudinal stretch. (*e*) Longitudinal true stress. (*f*) Latitudinal true stress.

definition $\lambda_2 = r/R$. Consequently, Eqs. (1), (2), (28), and (29) are the first-order ordinary differential equations that govern the four functions $r(R)$, $z(R)$, $\theta(R)$, and $\lambda_1(R)$.

The four first-order differential equations, along with the boundary conditions, are solved by using the shooting method. The active membrane and the passive membrane are computed separately. For the passive membrane pressed by the punch, the radius of contact B is prescribed, the force F, as well as b and h, are calculated as part of the solution to the boundary-value problem.

The fluid is taken to be incompressible. As the membranes deform, the volume of the fluid sealed between the membranes remains constant at a prescribed value, $2V_0$. Consequently, the pressure p is to be determined, rather than given. In the calculation, however, we prescribe a pressure p to calculate all the fields by solving the differential equations with the boundary conditions. Subsequently, the volume enclosed by the membranes can be calculated. We vary the pressure p until the volume equals the prescribed value $2V_0$. In presenting computational results, we indicate the amount of the sealed fluid by using the height h_0 of the apex of a membrane when the actuator is in the rest state, Fig. 3(*c*).

6 Computational Results and Discussions

To be consistent with the experimental parameters listed in Table 1, in calculation we set the prestretch as $a/A = 4$, and the normalized apical height in the rest state as $h_0/A = 0.712$. We normalize the pressure as $p/(\mu H/A)$, the voltage as $\Phi/\left(H\sqrt{\mu/\varepsilon}\right)$, and the force as $F/(\mu AH)$.

When the HCDE actuators are developed as Braille displays, it is desirable to reduce the voltage to actuate. Figure 5(*a*) plots the voltage applied to the bottom membrane as a function of the apical displacement of the top membrane. The experimental data taken from Ref. [14] correspond to the actuated state, Fig. 2(*b*). As the voltage ramps up, the bottom membrane expands in area and moves downward. Through the coupling of the fluid, the top membrane also moves downward. The only adjustable parameter in the calculation is $\sqrt{\mu/\varepsilon}$. This parameter is found to be $\sqrt{\mu/\varepsilon} = 1.73 \times 10^7$ V/m for the computational results to best fit the experimental data.

The elastomer used in the experiment is VHB 4910 (one kind of acrylic foam tapes fabricated by 3M Company), and the measured permittivity is $\varepsilon = 4.7\varepsilon_0$, where $\varepsilon_0 = 8.85 \times 10^{-12}$ F/m [33]. This value of the permittivity, along with our fitted parameter $\sqrt{\mu/\varepsilon} = 1.73 \times 10^7$ V/m, gives the shear modulus $\mu = 12.5$ kPa.

When the HCDE actuators are developed as Braille displays, it is desirable to increase the blocking force, and make the actuator relatively stiff in the rest state. Figure 5(*b*) plots the blocking force as a function of the apical displacement. The experimental data taken from Ref. [14] correspond to the voltage-off state, Fig. 2(*d*). The only adjustable parameter in this calculation is the shear modulus μ. We find $\mu = 15.0$ kPa for the computational results to best fit the experimental data.

Both Figs. 5(*a*) and 5(*b*) show excellent agreement between the computational results and experimental data. The agreement of the values of the shear modulus obtained from the above two estimates is satisfactory, given the uncertainty caused by representing the elastomer with the neo-Hookean model, and by the pronounced viscoelasticity of the material.

Figure 5(*c*) plots the pressure in the fluid as a function of the apical displacement of the top membrane. When the bottom membrane is subject to voltage, the pressure in the fluid lowers as the voltage ramps up. By contrast, when the top membrane is pressed by the punch, the pressure in the fluid rises as the punch moves down. Both trends are expected from physical considerations; however, at this writing, we do not have reliable experimental data to compare with these computational results. Incidentally, the pressure in the fluid can be determined by Eq. (13) once the force on the punch and the radius of contact are simultaneously measured in the experiment.

Dielectric elastomers are prone to several mechanisms of failure, including loss of tension, rupture by stretching, and electrical breakdown. One is therefore interested in various fields in the active membrane, Fig. 6. As the voltage increases, the active membrane expands its area and pulls the passive membrane down through the hydrostatically coupling effect, Figs. 6(*a*) and 6(*b*) shows that the true electric field in whole active membrane increases with the increase of the voltage. When the voltage becomes larger and larger, the true electric field at the center of the active membrane increases most dramatically. Assume that electrical breakdown occurs when the true electric field exceeds a critical value. We expect that the electric breakdown will occur at the center of the active membrane when the voltage is too high. As the voltage ramps up, stretches in the active membranes increase, Figs. 6(*c*) and 6(*d*), but the stresses decrease, Figs. 6(*e*) and 6(*f*). At all levels of the voltage, the stretches are the largest at the apex of the membrane.

For an actuator blocked by the punch, Fig. 7(*a*) shows the change in the shape of the actuator as the radius of contact increases. As the force on the punch ramps up, the radius of contact increases, and the coupling fluid transfers the downward motion to the bottom membrane. Figure 7(*b*) plots the area of contact as a function of the apical displacement.

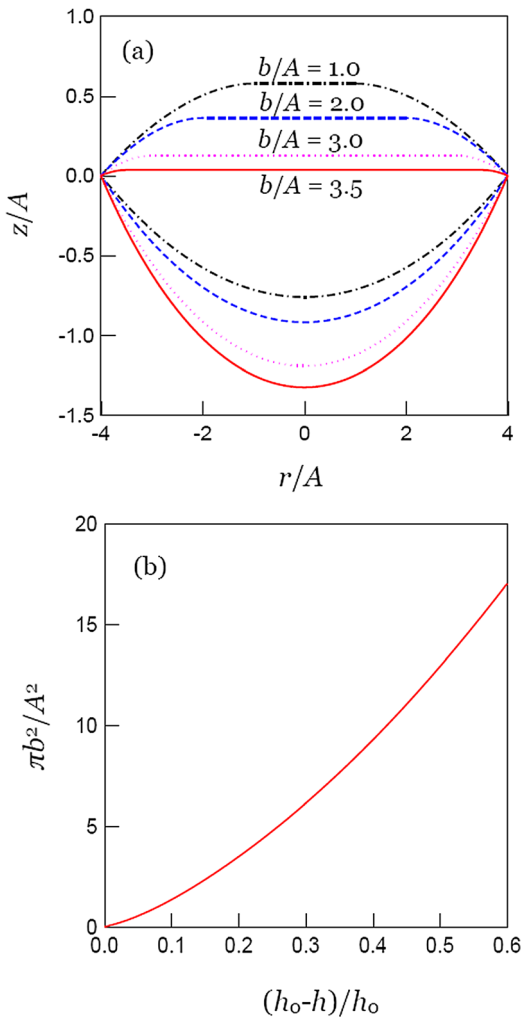

Fig. 7 While the voltage is off, a rigid flat punch is pressed onto the top membrane. (*a*) The deformed shapes of the actuator at several values of the radius of contact. (*b*) The normalized area of contact as a function of the normalized apical displacement.

7 Concluding Remarks

Mimicking muscles and bones, muscle-like actuators are often structures of tensegrity, with membranes of soft materials in tension and members of hard materials in compression. The inclusion of fluids in the structures imparts additional properties. The computational model described here can be used to predict strokes and blocking forces, optimize them by surveying the parameter space and analyze inhomogeneous fields to avert various modes of failure. We have also used the computational model to explore highly nonlinear behavior. For example, the model has predicted that, when the volume of the fluid exceeds a critical value, a HCDE actuator can break symmetry and be in one of two states of equilibrium. The two states are stable in the absence of the voltage and the force. One state can be switched to the other by applying either a voltage or a force. We have confirmed this bistable behavior experimentally and will report this intriguing development soon.

Acknowledgment

The work at Harvard is supported by the NSF through a grant on Soft Active Materials (CMMI–0800161), and by the MURI through a contract on Adaptive Structural Materials (W911NF-09-1-0476). H.M.W. is supported by Zhejiang University through the Xinxing Plan and China Scholarship Council as a visiting scholar at Harvard University, and by the National Natural Science Foundation of China (Grant No. 10872179), and by the Fundamental Research Funds for the Central Universities. F.C. would like to acknowledge financial support from the European Commission, in the framework of the projects "CEEDS: The Collective Experience of Empathic Data Systems" (FP7-ICT-2009.8.4, Grant 258749) and "VIACTORS: Variable Impedance Actuation Systems Embodying Advanced Interaction Behaviours" (FP7-ICT-2007-3, Grant 231554), and from COST (European Cooperation in Science and Technology), in the framework of "ESNAM: European Scientific Network for Artificial Muscles" (COST Action MP1003), for networking activities, which have contributed to the conception of this work.

References

[1] Pelrine, R., Kornbluh, R., Pei, Q. B., and Joseph, J., 2000, "High-Speed Electrically Actuated Elastomers With Strain Greater Than 100%," Science, **287**, pp. 836–839.
[2] Carpi, F., Rossi, D. D., Kornbluh, R., Pelrine, R., and Sommer-Larsen, P., 2008, *Dielectric Elastomers as Electromechanical Transducers: Fundamentals, Materials, Devices, Models and Applications of an Emerging Electroactive Polymer Technology*, Elsevier, Oxford.
[3] Brochu, P., and Pei, Q. B., 2010, "Advances in Dielectric Elastomers for Actuators and Artificial Muscles," Macromol. Rapid Commun., **31**, pp. 10–36.
[4] Carpi, F., Bauer, S., and Rossi, D. D., 2010, "Stretching Dielectric Elastomer Performance," Science, **330**, pp. 1759–1761.
[5] Suo, Z. G., 2010, "Theory of Dielectric Elastomers," Acta Mech. Solida Sinica, **23**, pp. 549–578.
[6] Cheng, A., 2011, "ViviTouch™ Offers a New Sensory Dimension to Mobile Gaming," WW-EAP Newsletter, **13**, pp. 2–2.
[7] Kofod, G., Wirges, W., Paajanen, M., and Bauer, S., 2007, "Energy Minimization for Self-Organized Structure Formation and Actuation," Appl. Phys. Lett., **90**, p. 081916.
[8] Zhao, X. H., and Suo, Z. G., 2010, "Theory of Dielectric Elastomers Capable of Giant Deformation of Actuation," Phys. Rev. Lett., **104**, p. 178302.
[9] Koh, S. J. A., Li, T. F., Zhou, J. X, Zhao, X. H., Hong, W., Zhu, J., and Suo, Z. G., 2011, "Mechanisms of Large Actuation Strain in Dielectric Elastomers," J. Polym. Sci., Part B: Polym. Phys., **49**, pp. 504–515.
[10] Rudykh, S., Bhattacharya, K., and deBotton, G., 2011, "Snap-Through Actuation of Thick-Wall Electroactive Balloons," Int. J. Non-Linear Mech., available at: http://dx.doi.org/10.1016/j.ijnonlinmec.2011.05.006.
[11] Keplinger, C., Li, T. F., Baumgartner, R., Suo, Z., and Bauer, S., 2012, "Harnessing Snap-Through Instability in Soft Dielectrics to Achieve Giant Voltage-Triggered Deformation," Soft Matter, **8**, pp. 285–288.
[12] Carpi, F., Frediani, G., and Rossi, D. D., 2010, "Hydrostatically Coupled Dielectric Elastomer Actuators," IEEE/ASME Trans. Mechatron., **15**, pp. 308–315.
[13] Carpi, F., Frediani, G., Tarantino, S., and Rossi, D. D., 2010, "Millimetre-Scale Bubble-Like Dielectric Elastomer Actuators," Polym. Int., **59**, pp. 407–414.
[14] Carpi, F., Frediani, G., Nanni, M., and Rossi, D. D., 2011, "Granularly Coupled Dielectric Elastomer Actuators," IEEE/ASME Trans. Mechatron., **16**, pp. 16–23.
[15] Yu, Z. B., Yuan, W., Brochu, P., Chen, B., Liu, Z. T., and Pei, Q. B., 2009, "Large-Strain, Rigid-to-Rigid Deformation of Bistable Electroactive Polymers," Appl. Phys. Lett., **95**, p. 192904.
[16] Goulbourne, N., Mockensturm, E., and Frecker, M., 2005, "A Nonlinear Model for Dielectric Elastomer Membranes," J. Appl. Mech., **72**, pp. 899–906.
[17] He, T. H., Zhao, X. H., and Suo, Z. G., 2009, "Dielectric Elastomer Membranes Undergoing Inhomogeneous Deformation," J. Appl. Phys., **106**, p. 083522.
[18] Zhao, X. H., and Suo, Z. G., 2008, "Method to Analyze Programmable Deformation of Dielectric Elastomer Layers," Appl. Phys. Lett., **93**, p. 251902 (the user-supplied subroutine for ABAQUS is available at http://imechanica.org/node/4234).
[19] O'Brien, B., McKay, T., Calius, E., Xie, S., and Anderson, I., 2009, "Finite Element Modeling of Dielectric Elastomer Minimum Energy Structures," Appl. Phys. A, **94**, pp. 507–514.
[20] Zhu, J., Cai, S. Q., and Suo, Z. G., 2010, "Resonant Behavior of a Membrane of a Dielectric Elastomer," Int. J. Solids Struct., **47**, pp. 3254–3262.
[21] Toupin, R. A., 1956, "The Elastic Dielectric," J. Rational Mech. Anal., **5**, pp. 849–914.
[22] Eringen, A. C., 1963, "On the Foundations of Electroelastostatics," Int. J. Eng. Sci., **1**, pp. 127–153.
[23] Tiersten, H. F., 1971, "On the Nonlinear Equations of Thermoelectroelasticity," Int. J. Eng. Sci., **9**, pp. 587–604.
[24] Bhattacharya, K., Li, J., and Xiao, Y., 2001, "Electro-Mechanical Models for Optimal Design and Effective Behavior of Electro-Active Polymers," *Electroactive Polymer (EAP) Actuators as Artificial Muscles. Reality, Potential and Challenges*, Y. Bar-Cohen ed., SPIE Press, Bellingham, WA, pp. 309–330.
[25] McMeeking, R. M., and Landis, C. M., 2005, "Electrostatic Forces and Stored Energy for Deformable Dielectric Materials," J. Appl. Mech., **72**, pp. 581–590.
[26] Dorfmann, A., and Ogden, R. W., 2005, "Nonlinear Electroelasticity," Acta Mech., **174**, pp. 167–183.
[27] Plante, J. S., and Dubowsky, S., 2006, "Large-Scale Failure Modes of Dielectric Elastomer Actuators," Int. J. Solids Struct., **43**, pp. 7727–7751.
[28] Wissler, M., and Mazza, E., 2007, "Mechanical Behavior of an Acrylic Elastomer Used in Dielectric Elastomer Actuators," Sens. Actuators, A, **134**, pp. 494–504.
[29] Zhao, X. H., Hong, W., and Suo, Z. G., 2007, "Electromechanical Coexistent States and Hysteresis in Dielectric Elastomers," Phys. Rev. B, **76**, p. 134113.
[30] Vu, D. K., Steinmann, P., and Possart, G., 2007, "Numerical Modeling of Non-Linear Electroelasticity," Int. J. Numer. Methods Eng., **70**, pp. 685–704.
[31] Trimarco, C., 2009, "On the Dynamics of Electromagnetic Bodies," Int. J. Adv. Eng. Sci. Appl. Math., **1**, pp. 157–162.
[32] Long, R., Shull, K. R., and Hui, C. Y., 2010, "Large Deformation Adhesive Contact Mechanics of Circular Membranes With a Flat Rigid Substrate," J. Mech. Phys. Solids, **58**, pp. 1225–1242.
[33] Kofod, G., Sommer-Larsen, P., Kornbluh, R., and Pelrine, R., 2003, "Actuation Response of Polyacrylate Dielectric Elastomers," J. Intell. Mater. Syst. Struct., **14**, pp. 787–793.
[34] Treloar, L. R. G., 1975, *The Physics of Rubber Elasticity*, Oxford University Press, Oxford.
[35] Lochmatter, P., Kovacs, G., and Michel, S., 2007, "Characterization of Dielectric Elastomer Actuators Based on a Hyperelastic Film Model," Sens. Actuators, A, **135**, pp. 748–757.
[36] Leng, J. S., Liu, L. W., Liu, Y. J., Yu, K., and Sun, S. H., 2009, "Electromechanical Stability of Dielectric Elastomers," Appl. Phys. Lett., **94**, p. 211901.
[37] Diaz-Calleja., R., and Llovera-Segovia, P., 2010, "Energy Diagrams and Stability Restrictions for Electroelastic Generators," J. Polym. Sci. B, **48**, pp. 2023–2028.
[38] Xu, B.-X., Mueller, R., Classen, M., and Gross, D., 2010, "On Electromechanical Stability Analysis of Dielectric Elastomer Actuators," Appl. Phys. Lett., **97**, p. 162908.
[39] De Tommasi, D., Puglisi, G., Saccomandi, G., and Zurlo, G., 2010, "Pull-In and Wrinkling Instabilities of Electroactive Dielectric Actuators," J. Phys. D: Appl. Phys., **43**, p. 325501.
[40] Bertoldi, K., and Gei, M., 2011, "Instabilities in Multilayered Soft Dielectrics," J. Mech. Phys. Solids, **59**, pp. 18–42.